

## MICROLENSING DETECTIONS OF MOONS OF EXOPLANETS

CHEONGHO HAN

Program of Brain Korea 21, Department of Physics, Chungbuk National University, Chongju 361-763, Korea;  
 cheongho@astroph.chungbuk.ac.kr

*Submitted to The Astrophysical Journal*

### ABSTRACT

We investigate the characteristic of microlensing signals of Earth-like moons orbiting ice-giant planets. From this, we find that non-negligible satellite signals occur when the planet-moon separation is similar to or greater than the Einstein radius of the planet. We find that the satellite signal does not diminish with the increase of the planet-moon separation beyond the Einstein radius of the planet unlike the planetary signal which vanishes when the planet is located well beyond the Einstein radius of the star. We also find that the satellite signal tends to have the same sign as that of the planetary signal. These tendencies are caused by the lensing effect of the star on the moon in addition to the effect of the planet. We determine the range of satellite separations where the microlensing technique is optimized for the detections of moons. By setting an upper limit as the angle-average of the projected Hill radius and a lower limit as the half of the Einstein radius of the planet, we find that the microlensing method would be sensitive to moons with projected separations from the planet of  $0.05 \text{ AU} \lesssim d_p \lesssim 0.24 \text{ AU}$  for a Jupiter-mass planet,  $0.03 \text{ AU} \lesssim d_p \lesssim 0.17 \text{ AU}$  for a Saturn-mass planet, and  $0.01 \text{ AU} \lesssim d_p \lesssim 0.08 \text{ AU}$  for a Uranus-mass planet. We compare the characteristics of the moons to be detected by the microlensing and transit techniques.

*Subject headings:* gravitational lensing

### 1. INTRODUCTION

All planets in our solar system except Mercury and Venus have moons. With the increasing number of discovered extrasolar planets, the existence of moons and their characteristics in these exoplanets emerge as new questions. Several methods to answer these questions have been proposed. Sartoretti & Schneider (1999) pointed out that high-precision photometry of stars during planet transit can be used to detect extrasolar moons either by direct satellite transit or perturbation in the timing of the planet transit. Brown et al. (2001) applied this method to the transit planet HD 209458b and placed upper limits on moons orbiting the planet by using the transit light curve obtained from *Hubble Space Telescope* observations.

In addition to the transit method, microlensing technique can also be used for the detections of extrasolar moons. This possibility was first mentioned by Bennett & Rhie (2002). They claimed that space-based lensing surveys with high precision and cadence would be able to detect not only planets but also moons orbiting the planets. From the investigation of satellite-induced lensing signals, Han & Han (2002) pointed out that detections of Earth-Moon like systems would be difficult because the satellite signal would be seriously smeared out by severe finite source effect. However, moons with large masses may exist. From detailed investigation of the long-term dynamical stability of moons, Barnes & O'Brien (2002) pointed out that Earth-like moons of Jovian planets could have stable orbits for long time scales. If such massive moons are common, it will be possible to detect them by using the microlensing technique.

In this paper, we investigate the characteristics of the lensing signals of Earth-like moons orbiting ice-giant planets. We investigate the variation of satellite signals depending on the locations of satellites and masses and locations of host planets. We also determine the range of satellite separations where the microlensing technique is optimized for the detections of moons.

### 2. BASICS OF LENSING

For the description of the lensing behavior produced by satellite systems, it is required to include at least three lens components of the host star, planet, and moon. For a multiple-lens system, the image mapping from the lens plane to the source plane is expressed as

$$\zeta = z - \sum_{k=1}^N \frac{m_k/M}{\bar{z} - \bar{z}_{L,k}}, \quad (1)$$

where  $N$  is the number of the lens components,  $\zeta = \xi + i\eta$ ,  $z_{L,k} = x_{L,k} + iy_{L,k}$ , and  $z = x + iy$  are the complex notations of the source, lens, and image positions, respectively,  $\bar{z}$  denotes the complex conjugate of  $z$ ,  $m_k$  are the masses of the individual lens components,  $M = \sum_k m_k$  is the total mass of the system, and  $m_k/M$  represent the mass fractions of the individual lens components. Here all lengths are expressed in units of the Einstein radius that is related to the lens mass and the distances to the lens ( $D_L$ ) and source ( $D_S$ ) by

$$\begin{aligned} \theta_E &= \left( \frac{4GM}{c^2} \right)^{1/2} \left( \frac{1}{D_L} - \frac{1}{D_S} \right)^{1/2} \\ &\sim 0.55 \text{ mas} \left( \frac{M}{0.3 M_\odot} \right)^{1/2} \left( \frac{D_S}{8 \text{ kpc}} \right)^{-1/2} \left( \frac{D_S}{D_L} - 1 \right)^{1/2}. \end{aligned} \quad (2)$$

Due to lensing, the image of the source star is split into multiple fragments and the individual images are distorted. The fragmentation and distortion of the source image cause variation of the source brightness. The lensing process conserves the source surface brightness, and thus the magnification of each image corresponds to the ratio between the areas of the image and source. For an infinitesimally small source, the magnification of each image is obtained by the Jacobian of

the mapping equation, i.e.

$$A_i = \left| \left( 1 - \frac{\partial \zeta}{\partial \bar{z}} \frac{\partial \bar{\zeta}}{\partial z} \right)^{-1} \right|. \quad (3)$$

For Galactic lensing events, the typical separations between images are of the order of 0.1 mas and thus the individual images cannot be resolved. However, events can be noticed by the variation of the source star flux where the total magnification corresponds to the sum of the magnifications of the individual images, i.e.  $A = \sum_i A_i$ .

One important difficulty in describing the lensing behavior of a multiple lens system is that the mapping equation is expressed in terms of the source position as a function of the image and lens positions. This implies that finding image positions for a given source position requires inversion of the mapping equation but the inversion is algebraically impossible for a multiple lens system. One way to obtain the image positions is expressing the mapping equation as a polynomial in  $z$  and then numerically solving the polynomial (Witt & Mao 1995). The advantage of this method is that it enables semi-analytic description of the lensing behavior and saves computation time. However, the order of polynomial increases as  $N^2 + 1$  (Rhie 1997) and thus solving the polynomial becomes difficult as the number of lens components increases. In this case, one can still obtain the magnification patterns by using the inverse ray-shooting technique (Schneider & Weiss 1986; Kayser, Refsdal & Stabell 1986; Wambsganss, Paczyński & Schneider 1990). In this method, a large number of light rays are uniformly shot from the observer plane through the lens plane and then collected (binned) in the source plane. Then, the magnification pattern is obtained by the ratio of the surface brightness (i.e., the number of rays per unit area) on the source plane to that on the observer plane. Once the magnification pattern is constructed, the light curve resulting from a particular source trajectory corresponds to the one-dimensional cut through the constructed magnification pattern. Although this method requires a large amount of computation time for the construction of detailed magnification patterns, it has an important advantage that the lensing behavior can be investigated regardless of the number of lenses. In addition, one can easily incorporate the finite source effect, which is important for the description of the perturbations caused by low-mass objects such as planets and moons (Bennett & Rhie 1996). Due to this reason, we use the ray-shooting method for the investigation of magnification patterns.

Due to the small mass ratio of the planet and even smaller mass of the moon, the lensing light curve of an event produced by a star having a planet with moons is well described by the single-lens light curve produced by the host star for most of the event duration. A short-duration perturbation occurs when the planet happens to be at the location of one of the two images of the source star produced by the host star (Gaudi & Gould 1997). Since the moon is close to the planet, the moon can also perturb the image and produce an additional anomaly. The position of the image-perturbing planet in the lens plane corresponds to the position of caustic in the source plane. In other words, perturbations occur when the source is located close to the caustic. The caustic represents the set of positions in the source plane at which the magnification of a point source event is infinite. For the binary lens case composed of the star and planet, there exist two sets of

caustics. One is located very close to the star (central caustic) and the other is located away from the star (planetary caustic). Among the two perturbation regions around the individual caustics, noticeable perturbations induced by the moon are expected only in the region around the planetary caustic. Two factors cause difficulties in finding satellite signatures around the central caustic region. First, the central perturbation produced by the moon occurs in a very tiny region. As a result, the signature of the moon would be significantly washed out by the finite source effect. Second, the perturbation regions of the planet and the moon nearly coincide. Then, the anomaly in the lensing light curve would be dominated by that of the planet due to the overwhelming mass of the planet compared to the mass of the moon, making it even more difficult to identify the satellite signature. We therefore focus on the perturbation region around the planetary caustic throughout the paper.

The location of the planetary caustic is related to the star-planet separation by

$$\mathbf{s}_c = \mathbf{s}_p \left( 1 - \frac{1}{s_p} \right)^2, \quad (4)$$

where  $\mathbf{s}_p$  represents the position vector of the planet from the star and its length is normalized by the Einstein radius of the star. Then, the caustic is located on the planet side when the planet is outside the Einstein ring ( $s_p > 1.0$ ), while it is located on the opposite side when the planet is inside the ring ( $s_p < 1.0$ ). The number of caustics also depends on the planetary separation and it is one when  $s_p > 1.0$  and two when  $s_p < 1.0$ . The caustic is within the Einstein ring when the planetary separation is within the range of  $0.6 \lesssim s_p \lesssim 1.6$ . The caustic size, which is proportional to the chance of planetary perturbation, is maximized when the planet is in this region and thus this region is often called as ‘lensing zone’ (Gould & Loeb 1992). As the separation departs from the Einstein radius, the caustic becomes smaller as  $\propto s_p^{-2}$  for  $s_p \gg 1.0$  and  $\propto s_p^2$  for  $s_p \ll 1.0$ . In addition, the caustic size becomes smaller with the decrease of the planet/star mass ratio as  $\propto q_p^{1/2}$  (Han 2006). When the perturbation is produced by a planet located outside of the Einstein ring, the sign of the resulting anomaly in the lensing light curve is positive, implying that the magnification during the perturbation is higher than the corresponding magnification of the single lens event. On the other hand, if the perturbation is produced by a planet located outside of the ring, the sign of the anomaly is negative (Han & Chang 2003).

### 3. MAGNIFICATION PATTERN

We investigate the microlensing signals of an Earth-like moon around ice-giant planets. For this investigation, we construct magnification patterns of lens systems with physical parameters adopted from those of typical galactic microlensing events currently being detected toward the galactic bulge direction (Sumi et al. 2003; Udalski 2003). We assume that the planet-hosting star is located at a distance of  $D_L = 6$  kpc from the observer and has a mass of  $M_* = 0.3 M_\odot$ . We also assume that the source star is located at  $D_S = 8$  kpc, that corresponds to the distance to the Galactic center. Then the physical Einstein radius corresponding to the lens mass and distance is  $r_E = D_L \theta_E = 1.9$  AU. For the star-planet and planet-moon separations, we test various combinations keeping in mind that the planet-moon separation should have an upper limit. This upper limit is usually set by the Hill radius which approximates the gravitational sphere of influence of the planet in the

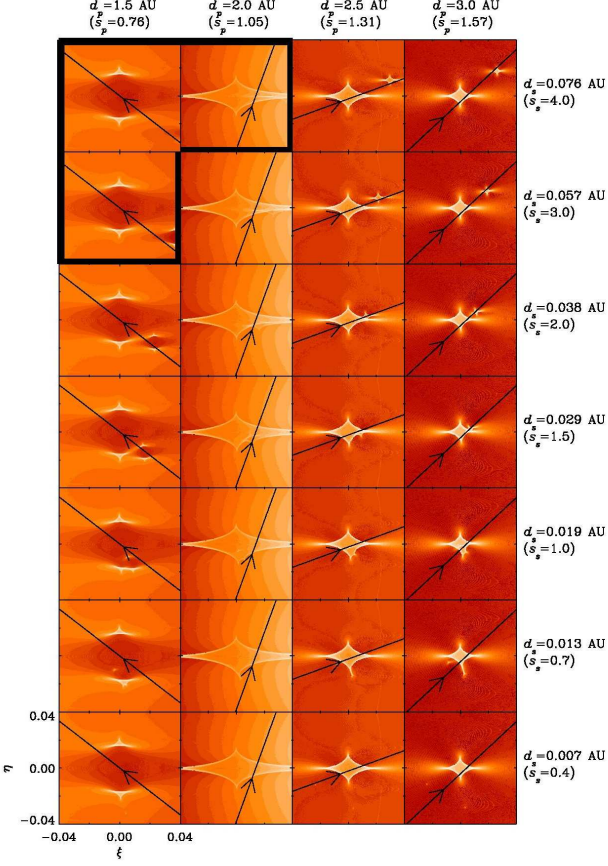


FIG. 1.— Magnification patterns of lens systems composed of a star, a planet, and a moon. The masses of the individual lens components are  $0.3 M_{\odot}$  for the star,  $10 M_E$  for the planet, and  $1.0 M_E$  for the moon. Each map is centered at the center of the planetary caustic produced by the planet. The moons have a common position angle of  $\phi = 60^\circ$  with respect to the star-planet axis, where the planet is located on the left. See Figure 2 for the geometry of the lens system. The labels above and on the right side represent the projected star-planet and planet-moon separations, respectively. The value in the parenthesis  $s_p$  represents the star-planet separation in units of the Einstein radius corresponding to the mass of the host star, while  $s_s$  represents the planet-moon separation normalized by the Einstein radius corresponding to the mass of the planet. Grey-scale is drawn such that brighter tone represents higher magnification. The panels blocked by thick solid lines represent the cases where the planet-moon separation is greater than the angle-average of the planet’s Hill radius. The light curves resulting from the source trajectories marked by straight lines with arrows in the individual panels are presented in the corresponding panels of Fig. 3.

face of the perturbation from the host star. The Hill radius is related to the semi-major axis,  $a$ , of the planet and the masses of the star,  $M_*$ , and planet,  $m_p$ , by

$$r_H = a \left( \frac{m_p}{3M_*} \right)^{1/3}. \quad (5)$$

Microlensing is only sensitive to the projected separation, while the 3-dimensional separation is important for the orbital stability. We, therefore, set the angle-average of the projected Hill radius, i.e.  $\sqrt{2/3}r_H$ , as the upper limit of the planet-moon separation. Since the satellite signal is an additional perturbation to the planet-induced perturbation, moons would be detected for events where planets are detected. We, therefore, test planets located within the lensing zone of the host star. In physical units, this corresponds to  $1.2 \text{ AU} \lesssim d_p \lesssim 3.0 \text{ AU}$ , where  $d_p$  is the projected star-planet separation.

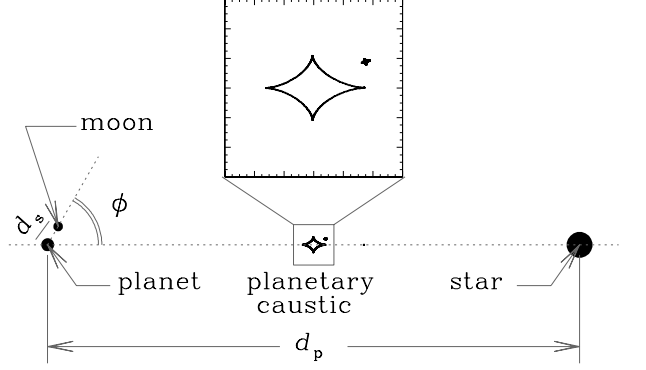


FIG. 2.— Geometry of the lens system composed of a star, a planet, and a moon. The area in the box represents the region where the magnification pattern is presented in Figure 1.

In Figure 1, we present the magnification patterns induced by a planet with moons of various projected separations from the planet. The planet has a mass of  $10 M_E$ , where  $M_E$  is the mass of the Earth. Each map is centered at the center of the planetary caustic produced by the planet. The moons have a common position angle of  $\phi = 60^\circ$  with respect to the star-planet axis, where the planet is located on the left. See Figure 2 for the geometry of the lens system. The labels above and on the right side of the maps represent the projected star-planet and planet-moon separations, respectively. The notations  $d_s$  and  $s_s$  represent the projected planet-moon separations expressed in physical units and in units of the Einstein radius corresponding to the mass of the planet,  $r_{E,p}$ , respectively. Grey-scale is drawn such that brighter tone represents higher magnification. The panels blocked by thick solid lines represent the cases where the planet-moon separation is greater than the angle-average of the projected Hill radius of the planet and thus moons are prohibited to reside. The light curves resulting from the source trajectories marked by straight lines with arrows in the individual panels are presented in the corresponding panels of Figure 3. For the construction of light curves, we take the finite-source effect into consideration by assuming that the source star has a radius of  $1.0 R_{\odot}$ .

From the magnification patterns and light curves, we find that non-negligible satellite signals occur when the planet-moon separation is similar to or greater than the Einstein radius of the planet, i.e.  $s_s \gtrsim 1.0$ . One thing to be noted is that the satellite signal does not diminish with the increase of the planet-moon separation beyond the Einstein radius of the planet. This contrasts to the planetary signal that vanishes when the planet is located well beyond the Einstein radius of the star. This is because although the lensing effect of the planet on the moon rapidly decreases with the increase of the planet-moon separation beyond  $r_{E,p}$ , the effect of the star on the moon remains. When, the planet-moon separation is substantially larger than the Einstein radius of the planet, the moon-induced perturbation forms at a separate region from the planet-induced perturbation region. In this case, the satellite signal on the light curve appears as a separate anomaly and thus it would be easily noticed. When  $s_s \sim 1.0$ , the perturbations induced by the planet and satellite interfere each other, resulting in complex magnification patterns. Then, although it would be still possible to notice the satellite signal, it would be sometimes difficult to unambiguously identify the

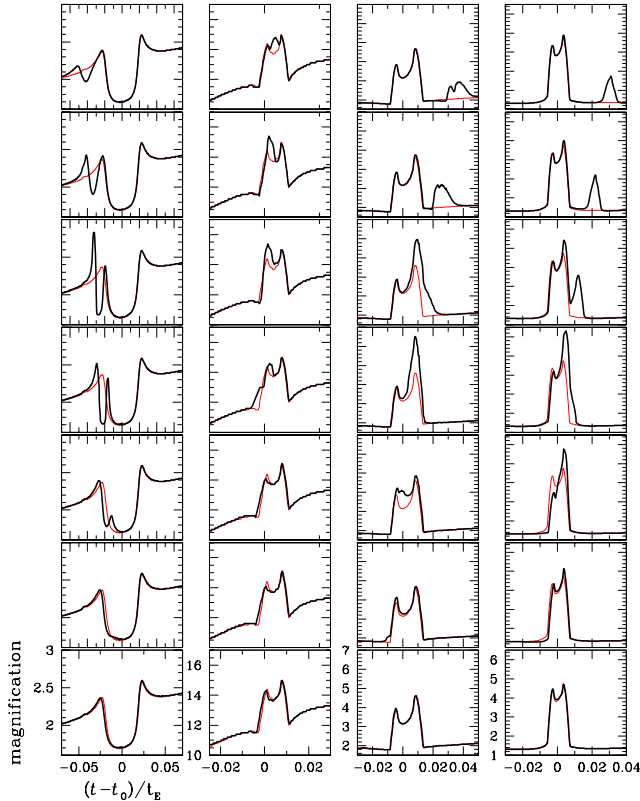


FIG. 3.— Light curves of lensing events produced by lens systems composed of a star, a planet, and a moon. The lens system geometry and source trajectories responsible for the individual events are presented in the corresponding panels of Fig. 1. In each panel, the thick and thin curves represent the light curves resulting from lens systems with and without the moon, respectively.

satellite signal. When the separation is substantially smaller than the planetary Einstein radius, the planet and moon behave as if they are a single component. In this case, it would be difficult to notice the satellite signal.

Another interesting trend of the satellite signal is that it tends to have the same sign as that of the planetary signal. This trend occurs because in most cases of identifiable moons with separations from the planet of  $s_p \gtrsim 1.0$ , the lensing effect of the host star on the moon is bigger than the effect of the planet. Then, the sign of the satellite perturbation is mostly determined by the star-moon separation. The star-moon separation is similar to the star-planet separation, and thus the sign of the planet-induced perturbation is same as that of the planet-induced perturbation.

We note that although the planet and moon often reveal themselves as separate signals, characterizing them from the independent analysis of the individual signals would be difficult. For some cases of triple lensing where the effect of the second body on the third body is negligible, it is possible to approximate the lensing behavior of the triple-lens system as the superposition of the two binary lens pairs composed of the first and second bodies and the first and third bodies. An example is the multiple-planetary system, where the lensing effect of a planet to another planet is negligible (Bozza 1999; Han et al. 2001). However, for the case of the star-planet-satellite system, the effect of the planet on the moon is usually not negligible and thus the approximation of binary superposition cannot be used for the analysis of the satellite signal.

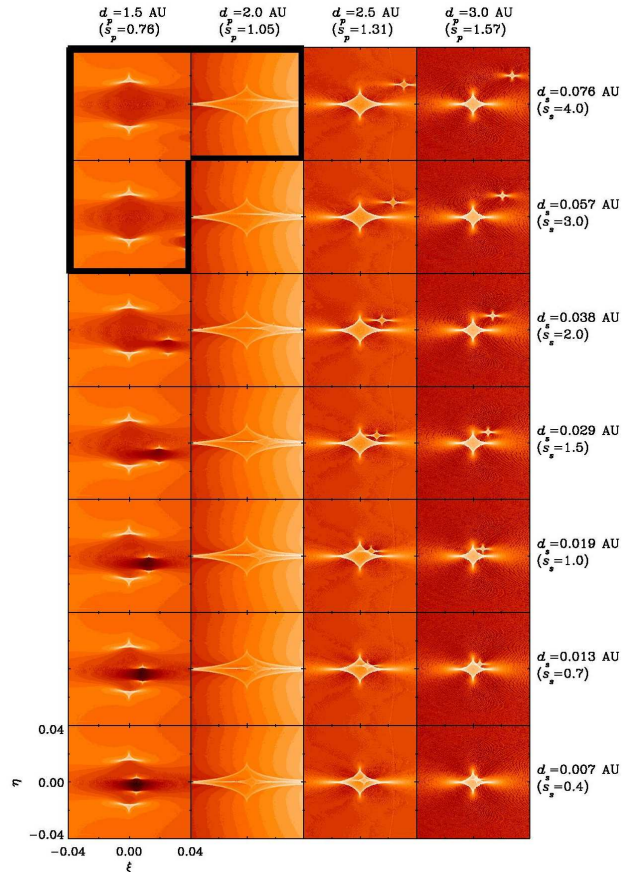


FIG. 4.— Magnification patterns of lens systems obtained by using the binary superposition approximation. Notations are same as in Fig. 1.

This can be seen from the comparison of the magnification patterns obtained by the exact triple-lensing formalism in Figure 1 and the patterns obtained by using the binary superposition approximation in Figure 4. As expected, it is found that the difference in the magnification patterns becomes larger as the planet-moon separation decreases.

Then, what will be the range of the satellite separation where the microlensing technique is optimized for the detections of moons. The lower limit of this range is set by the Einstein radius of the planet because moons with separations substantially smaller than  $r_{E,p}$  are hard to be detected. Since  $r_{E,p}$  depends on the planet's mass, planets with different masses have different lower limits. The upper limit is set by the Hill radius because moons cannot reside beyond  $r_H$ . The Hill radius depends not only on the planet mass but also on the star-planet separation. As a result, even planets with similar masses have different upper limits depending on where they are located in the system.

In Figure 5, we present the optimal range of satellite separations as a function of the star-planet separation for planets with different masses. We note that the labels of the star-planet separation on the bottom axis ( $s_p$ ) and the planet-moon separation on the left axis ( $s_s$ ) are expressed in units of the Einstein radii of the star and planet, respectively. The labels are expressed also in physical units on the top and right axes, respectively. The individual panels are for planets with masses of  $m_p = 300 M_E$ ,  $100 M_E$ , and  $10 M_E$ , which roughly corresponds to the masses of Jupiter, Saturn, and Uranus, re-

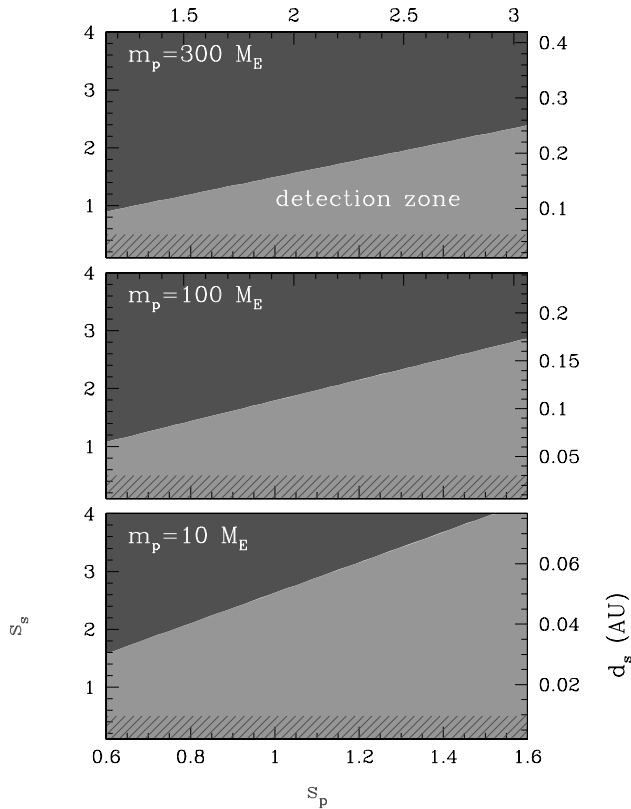


FIG. 5.— The optimal ranges of satellite separations where microlensing technique is sensitive to the detections of moons. The labels of the star-planet separation on the bottom axis ( $s_p$ ) and the planet-moon separation on the left axis ( $s_s$ ) are expressed in units of the Einstein radii of the star and planet, respectively. The labels on the top and right axes are expressed in physical units. In each panel, the light-shaded area represents the region of detectable satellites. The dark-shade area represents the region where the planet-moon separation is larger than the angle-average of the projected Hill radius of the planet and the hatched area represents the region where the separation is smaller than half of the planetary Einstein radius.

spectively. In each panel, the light-shaded area represents the region of detectable satellites. The dark-shaded area represents the region where the planet-moon separation is larger than the angle-average of the projected Hill radius and thus moons are prohibited to reside. The hatched area represents the region where the planet-moon separation is smaller than half of the Einstein radius of the planet and thus the satellite signal is hard to be detected. Although the range varies depending on the planet’s position in the stellar system, we find that the microlensing method would be sensitive to moons with separations from the planet of  $0.05 \text{ AU} \lesssim d_p \lesssim 0.24 \text{ AU}$  for a Jupiter-mass planet,  $0.03 \text{ AU} \lesssim d_p \lesssim 0.17 \text{ AU}$  for a Saturn-mass planet, and  $0.01 \text{ AU} \lesssim d_p \lesssim 0.08 \text{ AU}$  for a Uranus-mass planet.

#### 4. COMPARISON TO TRANSIT METHOD

Due to the uniqueness of the microlensing method in detecting planets and their moons, the characteristics of the moons to be detected by the microlensing method will be different from those to be discovered by the transit method. Below, we list some of these differences.

First, while the transit method can be used to search for moons of nearby stars, the microlensing method are sensitive to moons of remote stars. To meet the precision of photometry that is required to detect moons of extrasolar planets, the target stars of transit searches should be bright and thus they are

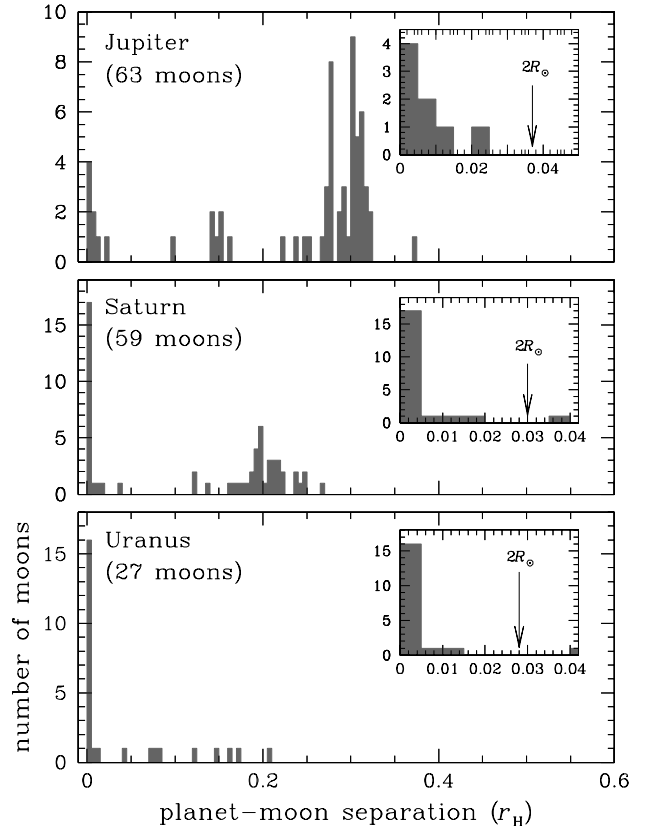


FIG. 6.— The semi-major axis distributions of the moons of Jupiter, Saturn, and Uranus. Note that the planet-moon separations are expressed in units of the Hill radii of the individual planets. The inset in each panel shows the distribution for close-in satellites to the planet. The arrow represents the upper limit of the planet-satellite separation for the detection of moons by using the transit method.

confined to the solar neighborhood. By contrast, microlensing searches are sensitive to stars anywhere along the line-of-sight toward the Galactic bulge. Therefore, the microlensing method can provide a sample of extrasolar moons distributed throughout the galaxy.

Second, while the transit method is most sensitive to moons of close-in planets, the microlensing method is sensitive to moons of planets in the region beyond the ‘snow line’. The snow line is the point in the protoplanetary disk beyond which the temperature is less than the condensation temperature of water (Lecar et al. 2006). Enhanced surface density of solids helps the formation of cores of giant planets and thus giant planets are thought to form in the region immediately beyond the snow line. The giant planets in our solar system, which are located in this region, have numerous moons; 63 known moons for Jupiter, 59 for Saturn, and 27 for Uranus. On the contrary, there might be few moons in close-in planets due to the strong tidal effect of the host stars as suggested by the two innermost planets of Mercury and Venus in our solar system.

Third, while the transit method is sensitive to moons located close to their host planets, moons detectable by the microlensing method will have wide separations from the planets. In order to produce additional dips in transit light curves, moons should be located very close to their planets with separations equivalent to or less than the diameter of the host star. On the other hand, the sensitivity of microlensing method extends up to the Hill radius. For the case of giant planets in our solar

system, the numbers of moons with separations larger than  $0.1r_H$  are 54 (85.7% of the all known moons), 38 (64.4%), and 5 (18.5%) for Jupiter, Saturn, and Uranus, respectively. See the semi-major axis distributions of the moons of Jupiter, Saturn, and Uranus in Figure 6. In these planets, there also exist close-in moons with separations from the planets less than the diameter of the sun; 7 (11.1%), 19 (32.2%), and 17 (63.0%) for Jupiter, Saturn, and Uranus, respectively. However, it would be difficult to detect them by using the transit method because the star-planet separation is large and thus the probability of planet transit is very low.

#### 5. CONCLUSION

We investigated the characteristic of microlensing signals of Earth-like moons orbiting ice-giant planets. For this, we constructed magnification patterns of lens systems with various star-planet and planet-moon separations. From this investigation, we found that non-negligible satellite signals occur when the planet-moon separation is similar to or greater than the Einstein radius of the planet. We found that the satellite signal does not diminish with the increase of the planet-moon separation beyond the Einstein radius of the planet unlike the

planetary signal which vanishes when the planet is located well beyond the Einstein radius of the star. We also found that the satellite signal tends to have the same sign as that of the planetary signal. These tendencies are caused by the lensing effect of the star on the moon in addition to the effect of the planet. We determined the range of satellite separations where the microlensing technique is optimized for the detections of moons. By setting an upper limit as the angle-average of the projected Hill radius and a lower limit as half of the Einstein radius of the planet, we found that the microlensing method would be sensitive to moons with projected separations from the planet of  $0.05 \text{ AU} \lesssim d_p \lesssim 0.24 \text{ AU}$  for a Jupiter-mass planet,  $0.03 \text{ AU} \lesssim d_p \lesssim 0.17 \text{ AU}$  for a Saturn-mass planet, and  $0.01 \text{ AU} \lesssim d_p \lesssim 0.08 \text{ AU}$  for a Uranus-mass planet. We compared the characteristics of the moons to be detected by the microlensing and transit techniques.

This work was supported by the Astrophysical Research Center for the Structure and Evolution of the Cosmos (ARC-SEC) of Korea Science and Engineering Foundation (KOSEF) through Science Research Program (SRC) program.

#### REFERENCES

- Barnes, J. W., & O'Brien, D. P. 2002, *575*, 1087  
 Bennett, D. P., & Rhie, S. H. 1996, *ApJ*, 472, 660  
 Bennett, D. P., & Rhie, S. H. 2002, *ApJ*, 574, 985  
 Brown, T. M., Charbonneau, D., Gilliland, R. L., Noyes, R. W., & Burrows, A. 2001, *ApJ*, 552, 699  
 Bozza, V., 1999, *A&A*, 348, 311  
 Gaudi, B. S., & Gould, A. 1997, *ApJ*, 486, 85  
 Gould, A., & Loeb, A. 1992, *ApJ*, 486, 85  
 Han, C. 2006, *ApJ*, 638, 1080  
 Han, C., & Chang, K. 2003, *ApJ*, 597, 1070  
 Han, C., Chang, H.-Y., An, J. H., & Chang, K. 2001, *MNRAS*, 328, 986  
 Han, C., & Han, W. 2002, *ApJ*, 580, 490  
 Kayser, R., Refsdal, S., & Stabell, R. 1986, *A&A*, 166, 36  
 Lecar, M., Podolak, M., Sasselov, D., & Chiang, E. 2006, *ApJ*, 640, 1115  
 Rhie, S. H. 1997, *ApJ*, 484, 63  
 Sartoretti, P., & Schneider, J. 1999, *A&AS*, 134, 553  
 Schneider, P., & Weiss, A. 1986, *A&A*, 164, 237  
 Sumi, T., et al. 2003, *ApJ*, 591, 204  
 Udalski, A. 2003, *AcA*, 53, 291  
 Wambsganss, J., Paczyński, B., & Schneider P. 1990, *ApJ*, 358, L33  
 Witt, H. J., & Mao, S. 1995, *ApJ*, 447, L105